ORIGINAL RESEARCH

Functionalization of multi-walled carbon nanotube and its effect on shape memory behavior of nanocomposite based on thermoplastic polyurethane/polyvinyl chloride/multi-walled carbon nanotube (TPU/PVC/MWCNT)

Maryam Ehteramian[1] · Ismail Ghasemi[1] 🄳 · Hamed Azizi[1] · Mohammad Karrabi[1]

Abstract

Nanocomposites based on thermoplastic polyurethane/polyvinyl chloride/multi-walled carbon nanotubes were prepared by a solution method and their shape memory properties were studied. The blend ratios were 70/30, 60/40, and 50/50 (w/w) of thermoplastic elastomer polyurethane/polyvinyl chloride. To improve the dispersion of multi-walled carbon nanotubes, at 0.5% and 1% (wt), in polymer matrices, three-step chemical modifications were performed, including oxidation, chlorination and grafting of poly (ε-caprolactone) diol. The occurrence of surface modifications in MWCNTs was monitored using Fourier transform infrared spectroscopy, elemental analysis, scanning electron microscopy and thermal gravimetric analysis techniques. SEM micrographs revealed a good dispersion of MWCNTs in the polymer matrix due to better matrix-filler interactions compared to filler–filler interactions. The results showed that the main indices of shape memory behavior (shape fixity and shape recovery) of nanocomposite samples were affected by the polymer blend ratio, nanoparticle concentration and surface modification. Increasing the content of polyvinyl chloride led to reduced shape fixity and shape recovery, which was attributed to the lack of rigid structural nature of polyvinyl chloride. The presence of nanoparticles contributed to enhanced shape fixity and weaker shape recovery. This can be explained by lower polymer chain mobility in the presence of multi-walled carbon nanotubes. The reduction in chain mobility in nanocomposites reinforced by surface-modified multi-walled carbon nanotubes was more significant due to higher distribution efficiency of nano-scale fillers in the polymer matrix.

Keywords Polyurethane/polyvinyl chloride blend · Multi-walled carbon nanotube · Nanocomposite · Functionalization · Shape memory behavior

Introduction

Shape memory polymers (SMPs) are a new class of smart materials that can be extensively recovered after deformation through excitation by heat, electricity, magnetic fields, and light [1–3]. A permanent form of shape memory polymers can be achieved by chemical covalent bonds or physical intermolecular interactions. Temperature-responsive polymers are the most common type of SMPs, which are defined as the thermal transition temperature in the programming section. The programming section is processed in such a way that the permanent shape of the polymer sample changes and sets a temporary form. Only polymers containing hard and soft segments show memory behavior [4–6]. Thermal transition temperature is expressed as net points or hard segment by T_{perm} and molecular switches or soft segment by T_{trans}. Depending on the physical nature, including crystals, glassy domains, chain entanglements, or chemical cross-links of the samples, T_{trans} can be glass transition temperature (T_g) or melting temperature (T_m).

Although SMPs present many potential technical advantages over conventional metallic shape memory alloys, their low degree of stress recovery originating from their low stiffness is their main drawback [7]. The use of reinforcing fillers, at the nano- and micro-scales, and blending the polymer

✉ Ismail Ghasemi
  i.ghasemi@ippi.ac.ir

[1] Department of Polymer Processing, Iran Polymer and Petrochemical Institute, P.O. Box 14965/115, Tehran, Iran

matrix with compatible polymers are common approaches to overcome low stiffness in SMPs [8–10].

A compatible blend based on thermoplastic elastomer polyurethane/polyvinyl chloride blend (TPU/PVC) is a common choice to develop SMPs. Several reports can be found in the literature on the shape memory properties of such a blend [11–13]. Jeong et al. studied the effect of PVC content on the morphology and shape memory in the blend with segmented TPUs. Their results showed that PVC was miscible with TPU and the prepared blends reduced the hysteresis in a tensile test at shape memory properties [11]. Rashidi et al. found that having higher PVC content in the blend increases the extent of dissolution between the soft and rigid domains of TPU [12]. In another report, Jeong et al. observed that with the increase in PVC content, hysteresis in the repeated cyclic test was reduced [13].

Also, there are some efforts in using nanofillers such as nano-clays, carbon nanotubes, nanoplatelet graphene, and other inorganic fillers to improve the shape memory properties of miscible blends [14–18]. These nanoparticles not only improve the stiffness and mechanical properties of SMPs but also serve as fixed structures that effectively enhance the shape memory behaviors. However, the challenge in obtaining adequate dispersion of these particles in polymeric matrices creates some considerable limitations to their usage. It has been reported that during nanocomposite preparation, multi-walled carbon nanotubes (MWCNTs) tend to agglomerate due to their high surface area. The main approach to achieve desirable dispersion of MWCNTs in nanocomposites is through chemical functionalization [19, 20].

Our goal of this study was to investigate the shape memory properties of the nanocomposites based on PVC/TPU/MWCNT. To avoid agglomerations and enhance the dispersion of MWCNTs, chemical functionalization was performed using poly (ε-caprolactone) diol (PCL diol). Functionalization reactions were tracked using thermal gravimetric analysis (TGA), Fourier-transform infrared spectroscopy (FTIR), and elemental analysis. The best temperatures for thermal transition temperatures were examined by dynamic mechanical thermal analysis (DMTA). The effects of functionalization and the MWCNTs content on shape recovery and shape fixity of the nanocomposites were studied and discussed in detail.

Experimental

Materials

Thermoplastic polyurethane-based polyester, type A 3485 (Bayer, Germany) in pellet form and suspension polyvinyl chloride with K value 70 from Bandar Emam Petrochemical Industry (Iran) were used as polymer matrix. Poly(ε-caprolactone) diol (PCL diol, with number average molecular weight 1000 g/mol, hydroxyl No. 112 mg KOH/g with a melting point between 40 and 50 °C) was purchased from Solvay Interox Company. Heat stabilizer based on calcium stearate was provided by Reagens Co. Italy. MWCNT (diameter 8–15 nm, a surface area about 150–250 m^2/g, the length between 5 and 30 μm and purity ≥95%) was purchased from Notrino Co. All chemicals, including nitric acid (HNO$_3$), sulfuric acid (H$_2$SO$_4$), thionyl chloride (SOCl$_2$), dimethylformamide (DMF), and tetrahydrofuran (THF) were laboratory type with high degrees of purity and purchased from Merck Co. For modification of particles, 0.22 μm millipore polypropylene and 0.45 μm millipore polytetrafluoroethylene (PTFE) membranes were prepared from Sigma Aldrich.

Sample preparation

Oxidized carbon nanotube (MWCNT-COOH)

Figure 1 summarizes the modification steps of MWCNT surface schematically. The first step was to prepare oxidized MWCNTs. Before the oxidization process, 1 g of MWCNT was placed in a ceramic plate and put in an oven at a temperature of 400 °C (heating rate 10 °C/min) for 2 h. This was done to remove the amorphous carbon particles. This process has been used in the literature by Galiotis et al., Wang et al., and Chui et al. [21–23].

Thermally modified MWCNTs were added in a concentrated mixture of 60% HNO$_3$ (200 mL) and 95% H$_2$SO$_4$ (600 mL) with a 1:3 volume ratio. Next, the mixture was sonicated with a power of 100 W and the nominal frequency of 80 kHz for 5 h at room temperature, and after this time, approximately 1200 mL distilled water was added into the suspension (1:100 by volume) and kept at room temperature for 24 h. Then, MWCNTs were sedimented and left in a dilute acidic mixture, and some distilled water was added again, and these suspensions were heated to 70 °C and stirred for 6 h. The cooled suspension was filtered under vacuum and washed with 4000 mL distilled water until its pH reached 6.5. The filtered solids were collected with 0.22 μm millipore polypropylene membrane and dried in a vacuum oven at 80 °C overnight. The product of this step was labeled as MWCNT-COOH.

Acylation of MWCNT-COOH

The acid-treated samples (MWCNTs-COOH) were dispersed in SOCl$_2$/DMF mixture (20:1 by volume) in an ultrasonic bath under the nitrogen atmosphere for 10 min at ambient temperature. In this step, DMF played the role of catalyst. The resulting suspensions were refluxed in a temperature range of 65–70 °C for 36 h. Under this condition,
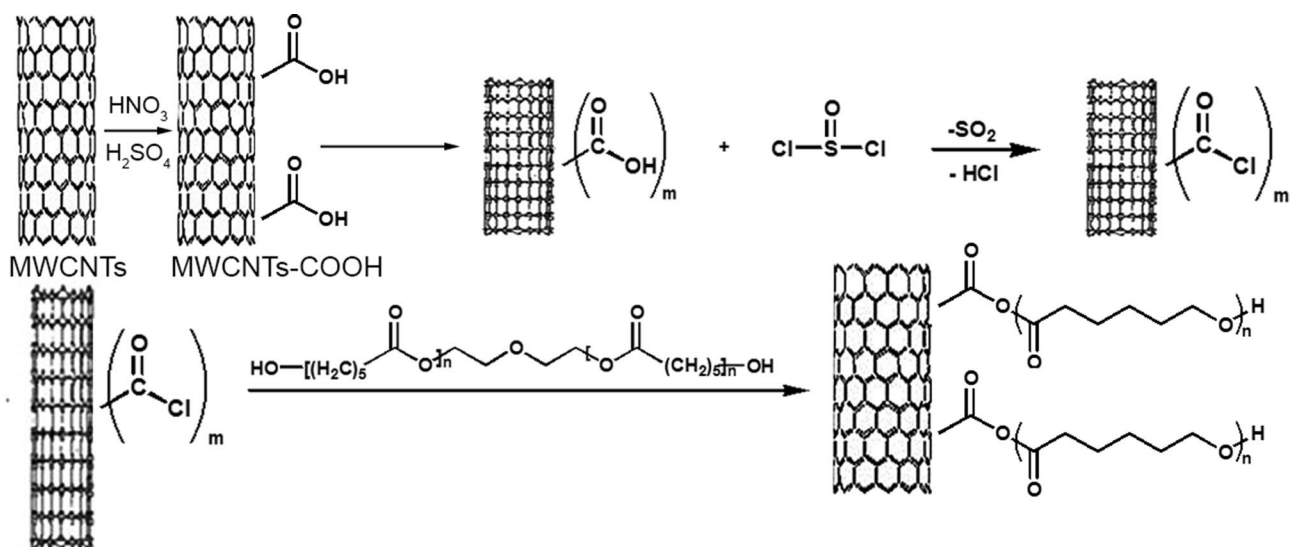
Fig. 1 Modification and grafting steps of MWNTs

the carboxyl groups were converted into acyl chlorides. To avoid a reverse reaction, sulfur dioxide (SO_2, as a by-product) was continuously removed [24]. By the completion of the reaction, the unreacted $SOCl_2$ was diluted with anhydrous THF, and the filtered powders under vacuum were washed three times with 150 mL anhydrous THF and dried in a vacuum oven for 2 h at 70 °C. Due to the high reactivity of –COCl groups, the obtained materials were kept away from humidity.

MWCNT-PCL

Before the reaction of PCL with MWCNT, the former was put into the vacuum oven at 40 °C for 2 h. Immediately, MWCNTs-COCl samples from the previous step were added into 20 mL dichlorobenzene and excess PCL. The suspension was refluxed under a magnetic stirring condition at 120 °C for 72 h. The obtained mixture was filtered through 0.45 μm millipore polytetrafluoroethylene (PTFE) membranes and washed with anhydrous THF to remove the ungrafted PCL. The samples were dried in a vacuum oven at 70 °C for 2 h [25].

Nanocomposite formation

Nanocomposites were prepared using the solution mixing method in THF. The pure MWCNTs, MWCNTs-COOH and MWCNTs-PCl were dispersed in THF using an ultrasonic bath for 30 min. The solution including PVC, TPU and calcium stearate as heat stabilizer was also prepared using THF. All materials were mixed for 30 min in an ultrasonic bath. To remove the excess solvent, the solutions were cast onto a clean glass plate and dried in the vacuum oven at 50–60 °C

for 12 h. The formulations of the samples are presented in Table 1. As can be seen, three blend ratios are selected and the nanoparticle concentrations are 0.5% and 1% (wt).

Characterization

The modification reactions on the surface of MWCNTs were studied by three methods, including FTIR, TGA, and elemental analysis. Transmission FTIR germanium crystal spectroscopy (Equinox 55 types, from Bruker Co., Germany) was used to evaluate the modification reactions of MWCNTs. The weight loss of raw MWNTs, before and after oxidation, and MWCNT-PCL degradation were monitored using a TGA1500 PL thermal analysis system at a heating rate 10 °C/min between 0 and 1000 °C under N_2 flow. Elemental analysis was obtained using a VarioEL (German) instrument to determine C, N, H, O elemental contents in MWCNTs samples.

Dynamic mechanical thermal analysis (DMTA) was employed to determine the glass transition temperature of the samples using TRITON-DMA, TRITEC 2000 DMA model. DMTA tests were carried out on rectangular specimens ($30 \times 10 \times 1$ mm) by applying a frequency of 1 Hz, the heating rate of 10 °C/min and scanning range from -100 to 100 °C.

A VEGA-II scanning electron microscope (Tescan, Czech) was conducted to study the morphology of the modified MWCNTs and nanocomposite samples. For MWCNT specimens, 1 mg of raw MWCNTs, MWCNT-COOH and MWNT-PCL were dispersed in 20 mL hydrous DMF by an ultrasonic probe with a power of 80 W for 20 min. One drop of the solution was put on an aluminum pillar. To study the morphology of the nanocomposites after etching in THF,

Table 1 Formulations of the nanocomposites samples

Sample code	PVC (wt%)	TPU (wt%)	Heat stabilizer (Phr)	MWCNTs (wt%)	MWCNTs-COOH (wt%)	MWCNTs-PCL (wt%)
S1	30	70	3	0	0	0
S2	40	60	3	0	0	0
S3	50	50	3	0	0	0
S4	40	59.5	3	0.5	0	0
S5	40	59.5	3	0	0.5	0
S6	40	59.5	3	0	0	0.5
S7	40	59	3	1	0	0
S8	40	59	3	0	1	0
S9	40	59	3	0	0	1
S10	50	49	3	0	0	1
S11	70	29	3	0	0	1

phr per hundred of polyvinyl chloride rubber

the samples were broken in liquid nitrogen after 10 min. The cryogenically fractured surface was coated with gold particles and observed by SEM.

Shape memory properties were induced through the cyclic thermal–mechanical method using a universal tensile machine, Instron 6022 equipped with a temperature-controlled chamber. The sheets were first heated from room temperature to above $T_g + 30$ °C with a preload force, and they were deformed to a temporary shape by 100% stretching. The samples under load were cooled below T_g by spraying liquid nitrogen rapidly for 10 min, while the temporary shape was fixed, and then the load was removed. The specimens were reheated, to above $T_g + 30$ °C for 15 min to allow the strain equilibrate. Then, the next cycle began ($N=2$), and the shape fixity (R_f %) and the shape recovery (R_r %) were recorded. The R_f and R_r, during thermomechanical cycles, were calculated by the equations given below [26]:

$$R_f = \frac{\varepsilon_u(N)}{\varepsilon_m} \times 100\% = \frac{L_i - L_0}{L_h - L_0} \times 100\% \quad (1)$$

$$R_r = \frac{\varepsilon_u - \varepsilon_p(N)}{\varepsilon_m - \varepsilon_p(N-1)} \times 100 = \frac{L_i - L_0(N)}{L_i - L_0(N-1)} \times 100 \quad (2)$$

In each thermomechanical cycle, the ratio of $\varepsilon_u(N)$ (strain on the stress-free state) to the maximum strain ε_m was defined by the rate of strain fixity (R_f %). $\varepsilon_u(N)$ is the difference between the new length L_i (after stress removal) and the permanent length (L_0). When the sample falls under the influence of heat and stress it forms a temporary shape (L_h). The maximum strain ε_m can be evaluated by differences between temporary shape and permanent length. For measuring the ability of the samples to recover their permanent shape (R_r), the restoring deformation was used to achieve the permanent shape in each cycle (ε_p). By removing the stress when heating the samples, the temporary length (L_i)

returned to a permanent length, and the samples of length L_h were deformed and suddenly shrank to L_i. Nevertheless, L_i was not the same as L_0 because in each cycle some dissipation occurred, which had not been reported before at all.

Results and discussion

Characterization of functionalized MWCNT

FTIR analysis

The FTIR spectra of pure and functionalized MWCNTs are shown in Fig. 2. As can be seen, for pure MWCNT, there are some peaks at 3432 cm^{-1} (stretching vibration of O–H groups) and peaks around 2922 and 2855 cm^{-1} (stretching vibrations of symmetric and asymmetric CH$_2$ groups) [27].

Moreover, the peak at 1642 cm^{-1} (C=C bond between wall to wall carbon atoms in multiwall carbon nanotubes) is attributed to contaminations during the production process
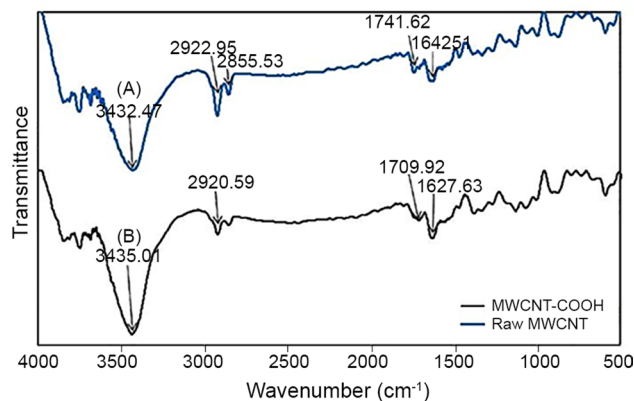

Fig. 2 FTIR spectra of: (**a**) pure MWCNT and (**b**) MWCNT-COOH

of MWCNT. By acid treatment, new peaks at 1709 and 1627 cm^{-1} appeared which can be assigned to C=O (carbonyl), and C–O is stretching mode in carboxylic groups. These peaks provide evidence of carboxylic groups present in MWCNTs, which have been reported by other researchers as well [25, 28, 29].

The FTIR spectra of MWCNT-COCL, neat PCL and MWCNT-PCL are also demonstrated in Fig. 3. As mentioned earlier, in acylation reaction using thionyl chlorides the carboxylic groups were converted to an acyl chloride (COCl). In comparison to MWCNT-COOH, a new peak was formed at 661 cm^{-1}, which can be assigned to C–Cl bond. In addition, the stretching vibration peaks of C=O and C–O shifted from 1709 and 1099 cm^{-1} to 1741 and 1118 cm^{-1}, respectively. These shifts in peaks may be related to greater electronegativity of chlorine compared to oxygen atom [30].

After grafting of PCL on MWCNT-COCl, a strong carbonyl bond was identified at 1732 and 1163 cm^{-1} (related to the ester groups in PCL) [13, 31]. A small and weak absorption peak was also seen at 721 cm^{-1} that was assigned to the bending vibration of (CH$_2$)$_n$ when $n \geq 4$ [32]. By comparing this spectrum with that of MWCNT-COCL, one can find that the grafting reaction has occurred on the surface of carbon nanotubes [24]. Similar results were observed in the works of other researchers [25, 29, 33].

TGA analysis

One of the most useful methods for quantitative analysis of surface modification of carbon nanotubes and measuring several organic materials that were grafted onto MWCNT is thermogravimetric analysis [34, 35]. The TGA thermograms of neat MWCNT, MWCNT-COOH, and MWCNT-PCL are
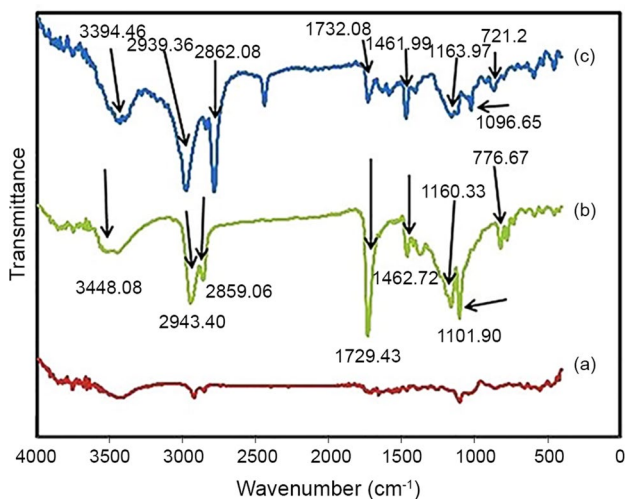
illustrated in Fig. 4. As can be seen, there is no considerable weight loss in neat MWCNT until the onset of thermal degradation temperature at 700 °C. However, a mass loss of about 0.75% (wt) is observed in a temperature range of 100–150 °C that can be attributed to low molecular weight impurities, amorphous carbon, and absorbed moisture [36, 37].

In modified carbon nanotubes, decomposition starts earlier than that of neat MWCNTs due to the presence of organic functional groups. In MWCNT-COOH, the weight loss is in the temperature range of 170–320 °C which is related to the degradation of the hydroxyl group [38]. It assumes that all the carboxylic groups have completely decomposed at about 320 °C. For MWCNT-PCL, on the other hand, there are two peaks below 500 °C. Similarly, the peak in the temperature range of 100–170 °C is related to humidity absorption at the surface of MWCNT-PCL. Another peak appears in the temperature range of 320–500 °C with slow steep corresponding to the PCL degradation. The same temperature range for degradation of PCL has been reported in the literature [18–20]. By comparing the TGA curves, one can find the maximum mass loss for 49% (wt) MWCNT-PCL relative to neat MWCNT and MWCNT-COOH (0.75% and 8% wt), respectively [39]. This significant difference can be
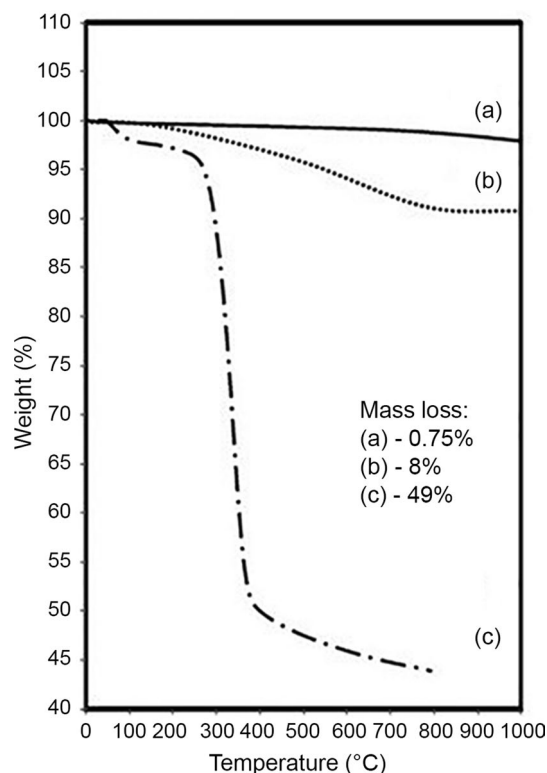
Fig. 3 FTIR spectra of: (**a**) MWCNT-COCL, (**b**) neat PCL and (**c**) MWCNT-PCL

Fig. 4 TGA thermograms: (**a**) pure MWCNT, (**b**) MWCNT-COOH and (**c**) MWCNT-PCL

an indication of the successful oxidation and grafting reactions in MWCNTs [40].

Elemental analysis

Elemental analysis was performed on MWCNTs, MWCNT-COOH and MWCNT-PCL to determine the main elements and their concentrations. The results are summarized in Table 2. The amount of carbon element and its corresponding ratios of nitrogen and oxygen is of particular importance because they are indications of oxidation and grafting reactions. The carbon content in neat MWCNT was 93.457% (wt), which decreased to 82.89% (wt) in MWCNT-COOH and 60% (wt) in MWCNT-PCL. On the other hand, the amount of oxygen was increased from 0 in pure MWCNT to 9.507% (wt) in MWCNT-COOH by acid treatment, suggesting the significant role of nitric/sulfuric acids as oxidative agents. After grafting with PCL, a further increase in oxygen content was observed and the oxygen content reached 30.179% (wt) in MWCNT-PCL. Besides, the increase of nitrogen in MWCNT-PCL may imply the existence of PCL on the carbon nanotube surface. The obtained results show that MWCNTs are successfully modified by acid treatment and grafting reaction.

Electron microscopy

Scanning electron microscopy was used to observe the physical conditions of MWCNT-COOH and MWCNT-PCL. Figure 5 shows SEM micrographs of the samples after modification accompanied by neat MWCNT for comparison at two magnifications (35k× and 75k×). As can be seen in Fig. 5, pure MWCNTs are mostly curved and entangled with cylindrical shapes. Some impurity particles are also observed, which may be attributed to metal catalytic and amorphous carbons produced during the synthesis process. After oxidation by H_2SO_4/HNO_3, all impurities were removed, leading to a shorter length of MWCNT and, some defects were formed on the sidewall and the tube ending [41]. It seems that, in the oxidation reaction, the long nanotubes are broken into the shorter open-ended tube and both ends and side walls are affected by an oxidation reaction.

No considerable changes were detected after the grafting reaction in comparison to MWCNT-COOH, which implies that the physical form of oxidized carbon nanotube was not affected by grafting reaction conditions [42].

Characterization of nanocomposites

Dynamic mechanical thermal analysis

DMTA test was done to determine the best temperature for thermal induction of shape memory properties. Also, the result of this test was used to evaluate the miscibility between PVC and TPU. Figure 6 depicts Tanδ versus temperature of the samples and, the obtained data are listed in Table 3. As can be seen in this figure, the $(Tanδ)_{max}$ values for raw TPU and PVC are -23.8 and 93.1 °C, respectively. With the blending of two polymers, just one $(Tanδ)_{max}$ was observed, which is an indication of good compatibility of two polymeric phases. With increasing PVC content, the maximum peak was shifted to higher temperatures.

The highest $(Tanδ)_{max}$ was related to the sample including 1%(wt) PCL-MWCNT which means that a strong interaction was formed between the nanoparticles and the polymer matrix. On the other hand, due to the appropriate interactions between the particles and the polymer chains, the chain movements are delayed, leading to a shift of $(Tanδ)_{max}$ to higher temperatures. In this research, 30 °C higher than $(Tanδ)_{max}$ was chosen as an extension temperature in the thermal programming of SMP.

Morphology

SEM was used to observe the morphology of the samples. Typical SEM micrographs of neat TPU/PVC 60/40 and samples containing MWCNT-COOH and MWCNT-PCL (0.5% (wt)) and the size distribution of dispersed phase are shown in Fig. 7. In these figures, the dark holes correspond to the PVC extraction. Our observation revealed that the dominant morphology is the droplet matrix for polymeric phases in the range of 2–15 μm. With increasing the TPU content, as the matrix, the particle size of the dispersed phase decreased. The main reason for this phenomenon maybe related to a decrease in the coalescence of the dispersed phase [43].

To achieve a better insight of the status of nanoparticles in the polymeric matrix, some SEM micrographs were obtained with higher magnifications (Fig. 8). The results

Table 2 Element analysis of neat MWCNT, MWCNTCOOH and MWCNT-P

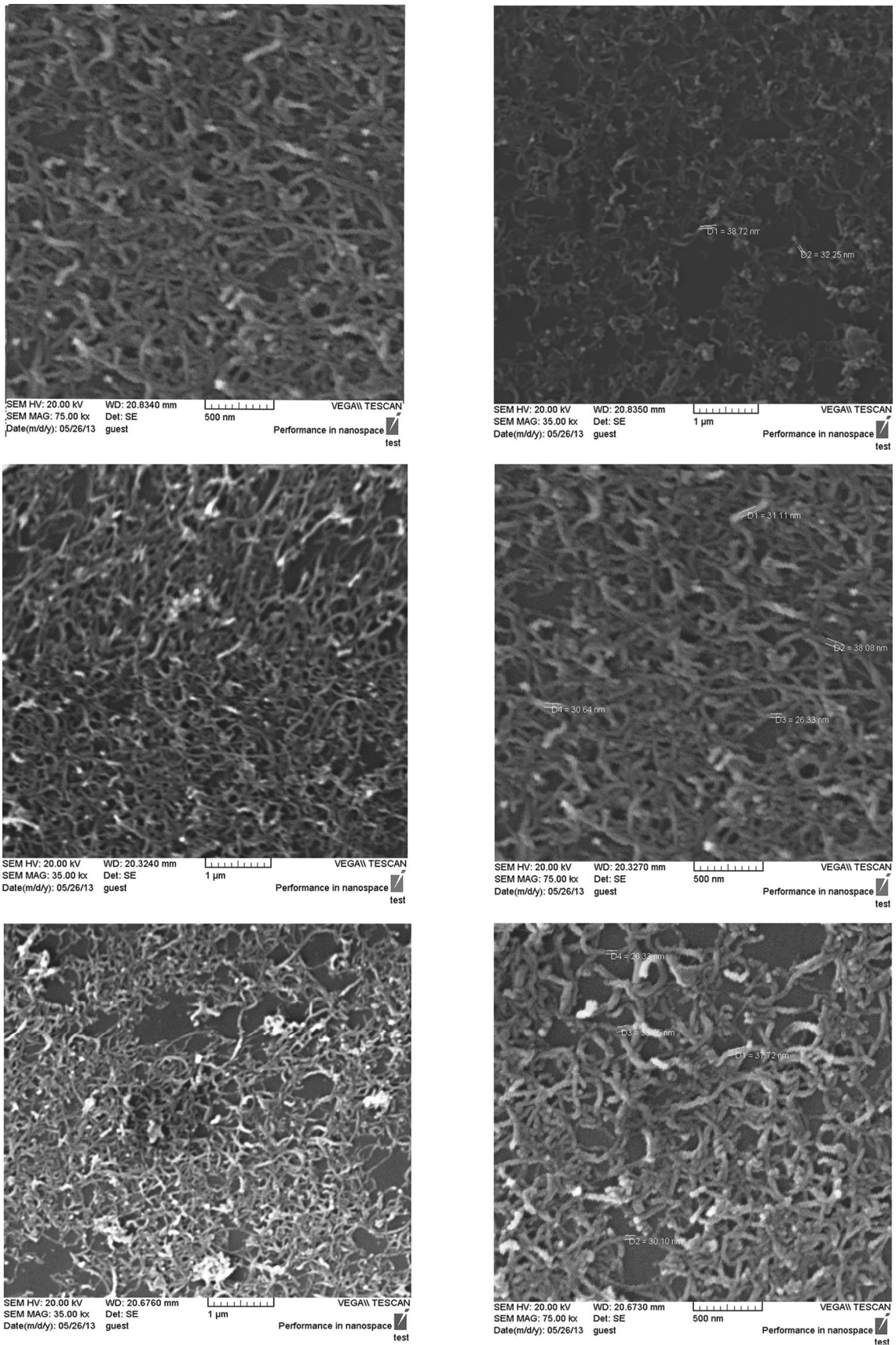| Sample	Oxygen (wt%)	Hydrogen (wt%)	Carbon (wt%)	Nitrogen (wt%)	Carbon/nitrogen ratio
Neat MWCNT	0	5.98	93.457	0.563	165.99
MWCNT-COOH	9.507	6.585	82.89	1.018	81.42
MWCNT-PCL	30.179	8.071	60	1.75	34.29

Fig. 5 SEM micrographs: (**a**) pristine MWCNT, (**b**) MWCT modified by acid and (**c**) MWCNT-PCL
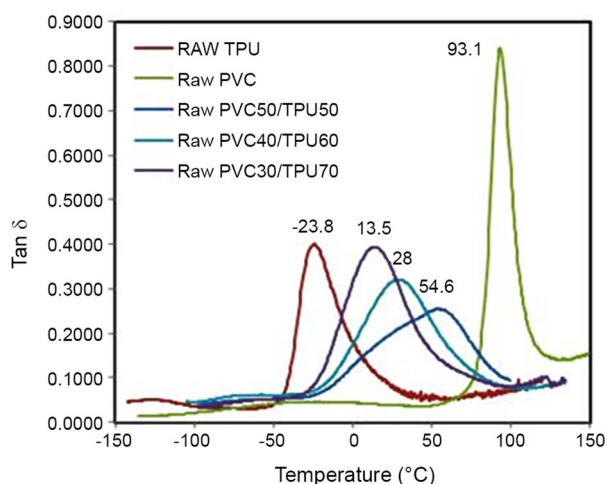
Fig. 6 Tanδ versus temperature of raw materials and neat blends

Table 3 Tan(δ)$_{max}$ of the samples

Sample	Tan(δ)$_{max}$ (°C)
S1	16
S2	28.5
S3	53.6
S4	29
S5	30
S6	30.5
S7	29.9
S8	30.4
S9	35
S10	54.5
S11	20.4

revealed better distribution and dispersion of nanoparticles, which was achieved in samples containing MWCNT-*g*-PCL due to superior interactions with polymer matrixes [44]. The existence of polar groups on the surface of the modified MWCNTs prevents their agglomerations while some agglomerations were observed in samples including neat MWCNTs. The measured sizes of nanoparticles in samples with modified MWCNTs are comparable with the reported pristine size.

Shape memory behavior

Shape fixity and shape recovery, as the main indices of a shape memory behavior, were determined and the results are summarized in Tables 4 and 5. All samples showed the above parameter in the range of 45–98.5%, which is acceptable for SMP materials. It was predicted that as the TPU content in the samples increased, R_r would increase and R_f would decrease. The increase in R_r was related to the flexible nature of TPU and the main reason for the reduction of R_f

was associated with the softer form of TPU at the extension temperature.

Contradictory results have been reported for shape fixity variation with nanofiller loading in the literature [45–47]. The fluctuation of shape fixity value is mainly affected by chain mobility. Any parameter that hinders chain mobility leads to a reduction in shape fixity. In our study, by incorporation of MWCNTs into the compound, R_f was increased. It seems that the presence of nanoparticles limited the soft segment movements of the polymeric chains and improved the shape fixity. R_r was also increased by the addition of nanoparticles due to the excellent stiffness of MWCNTs. It is well known that higher elastic modulus values lead to higher shape recovery [48, 49]. Gu et al. concluded that the elastic modulus ratio below and above the trigger temperature and the hard segment content play vital roles in shape memory behaviors, and that a high value of this ratio is of critical importance for appropriate shape memory performance [50].

The better performance was observed by the addition of modified MWCNTs. Both R_f and R_r were increased even more than those of samples containing neat MWCNTs. Because of the better interactions between the modified nanoparticles and the polymeric phases in these samples, there is a considerable limitation in the chain mobility, and therefore, an increase in the shape fixity. On the other hand, the better dispersion and distribution of nanoparticles in these samples produced greater reinforcement of the matrix, which means better elasticity properties and shape recovery. In other words, the stiffness and elasticity were improved upon the addition of modified MWCNTs accompanied by their prosperity dispersion in the matrix. This elasticity helped more energy to be stored in the temporary shape, and hence, higher shape recovery was achieved. Regarding Table 4, one can find that with an increase in the modified carbon nanotube concentration, R_f and R_r are enhanced.

Since the repeatability and consistency in the performance of SMPs materials are very important, the shape memory tests were performed in two cycles and the obtained data were compared with each other (Table 5). The results in Table 5 show that the shape fixity and recovery were lower in the second cycle in comparison to the first cycle for all samples. It assumes that in the second cycle of SMP tests, the plastic deformations of the soft segments of the polymers were intensified and resulted in lower shape fixity in the temporary shape. The main reason for the reduction of shape recovery can be attributed to lower hydrogen bonds in polymeric phases during two cycles of the test. Another probable reason for a reduction in shape recovery can be related to the disentanglement of the PVC phase in two cycles of the test. In other words, at the applied temperature and two-cycle tests, the possibility of opening of the entanglements at the fixing point for the PVC chains increases,
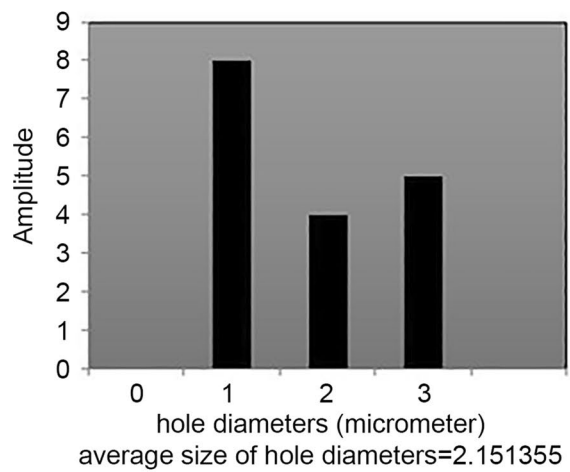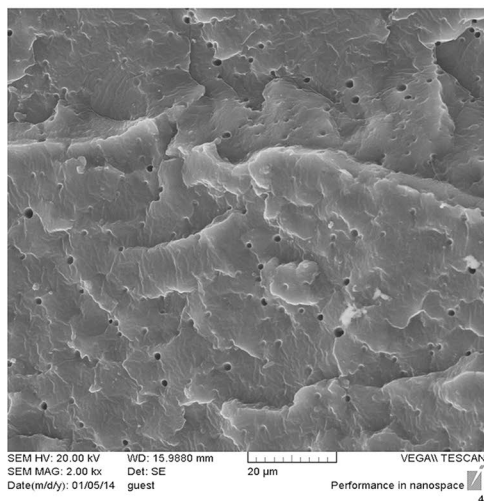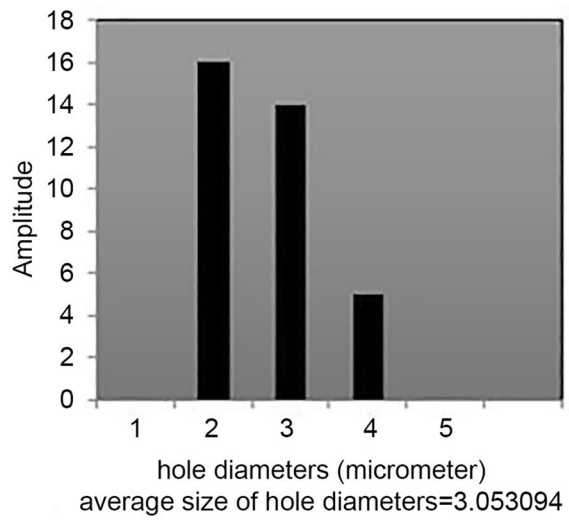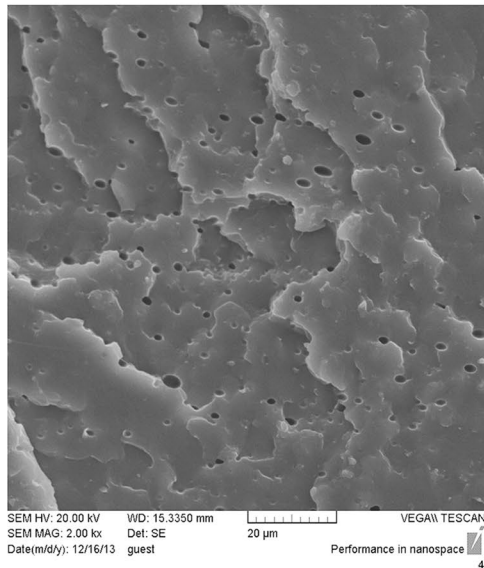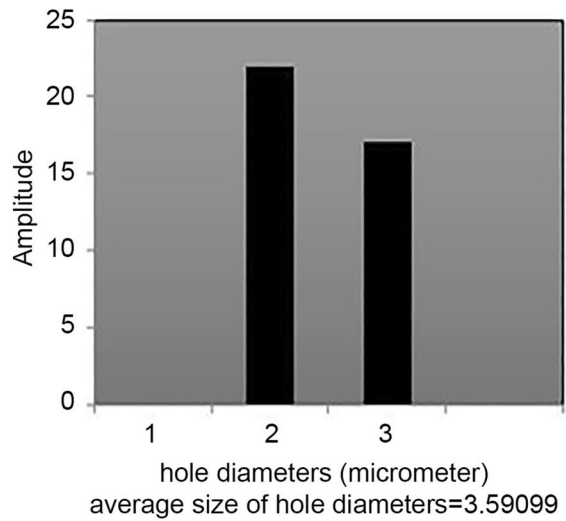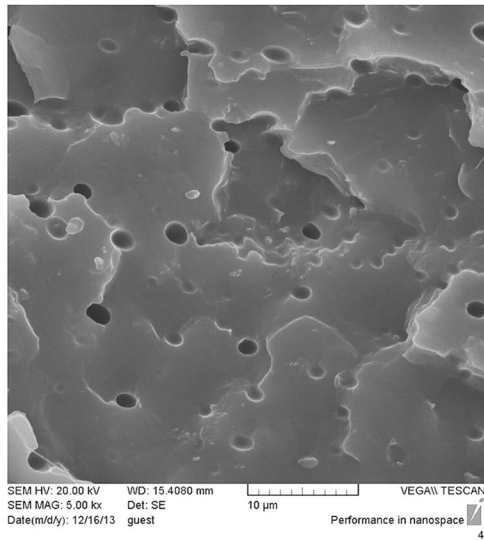
Fig. 7 Amplitude charts, SEM micrograph and distribution of dispersed phase for TPU60/PVC40 samples: (**a**) pure MWCNT (0.5% by wt) with 2000×, (**b**) MWCNT-COOH (0.5% by wt) with 2000× and (**c**) MWCNT-PCL (0.5% by wt) with 2000×
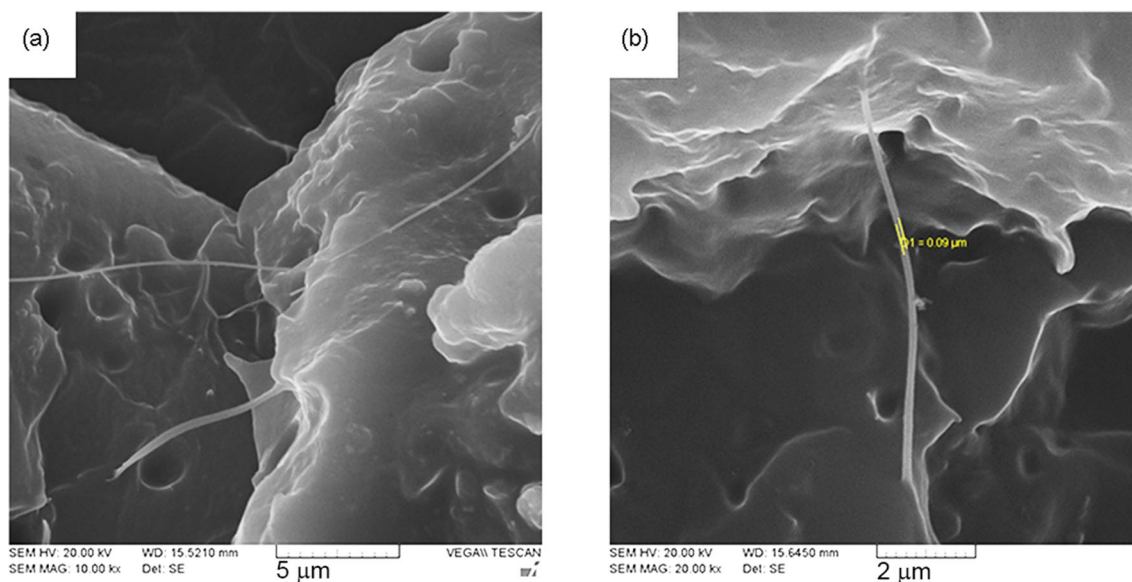
Fig. 8 SEM micrographs of TPU60/PVC40 blend including 0.5% (wt) MWCNT-PCL at higher magnifications

Table 4 Shape memory and shape recovery behavior for all samples in the first cycle

Sample	Shape fixity	Shape recovery (%)
S1	71	98.5
S2	64.34	97.94
S3	60	80
S4	71.91	91.64
S5	76.84	93.17
S6	87.36	95.61
S7	81.68	92.08
S8	88.5	95.55
S9	90.34	96
S10	91.70	82.84
S11	87.16	98.16

Table 5 Shape memory and shape recovery behavior for the blends and nanocomposites in the second cycle

Sample	Shape fixity	Shape recovery (%)
S1	68	95
S2	47.71	97.15
S3	45	76
S4	59.86	84.31
S5	67.16	88.23
S6	80.62	91.76
S7	71.36	85.84
S8	79.30	91.33
S9	83.7	92.94
S10	85.90	87.91
S11	78.90	97.91

and therefore fixity reduces. The reduction trend was changed by the incorporation of nanoparticles where the least reduction was observed for sample TPU/PVC 60/40 (wt/wt) MWCNT-*g*-PCL. In the second cycle, as the hard segments are under stress and can be covered by nanoparticles, therefore the applied stress can be tolerated by the nanoparticle instead of a hard segment. It means that the presence of nanoparticles prevents further lowering of the shape fixity and recovery by inhibiting the plastic deformation. The performance of modified MWCNTs in this manner is more efficient due to better dispersion in the matrix.

Conclusion

This study was motivated by current research works in the field of shape memory polymers based on polymer blends and nanocomposites. In this research, samples were prepared based on TPU/PVC/MWCNT by a solution method at different blend ratios of 70/30, 60/40, and 50/50 (w/w). By modification of the MWCNTs surface, the filler–matrix interactions were increased compared to the filler–filler interactions, resulting in better dispersion of nanoparticles. The formation of oxygen-containing groups during modification is the main reason for the increase in filler–matrix interactions.

The following results can be drawn from this work:

1. Characterization of modified MWCNTs by FTIR, elemental analysis and TGA methods showed successful modification reaction on MWCNTs.
2. SEM observations revealed the formation of good dispersion of nanoparticles in the polymer matrix and no changes in the structures and dimensions of nanoparticles. All particles retained their initial form during the three-step modification reactions.
3. In the DMTA thermograms, two different values of $(Tan\delta)_{max}$ were converted to a single temperature for PVC and TPU, which shows a good compatibility between the two polymer phases. The programming temperatures in the shape memory induction were selected around $(Tan\delta)_{max} + 30$ °C to involve the two polymers in the shape memory responses.
4. Evaluation of SEM photography at higher magnification compared the dispersion of neat MWCNT and the modified MWCNT surfaces. Modified nanoparticles showed highly superior dispersion in the TPU/PVC polymer matrix.
5. The best results for R_r and R_f indices were related to samples containing MWCNTs-PCL due to better dispersion and distribution of nanoparticles.

References

1. Ratna D, Karger-Kocsis J (2008) Recent advances in shape memory polymers and composites: a review. J Mater Sci 43:254–269
2. Meng Q, Hu J (2009) A review of shape memory polymer composites and blends. Compos A Appl Sci Manuf 40:1661–1672
3. Leng J, Du S (2010) Shape-memory polymers and multifunctional composites. CRC, New York
4. Suhas DP, Jeong HM, Aminabhavi TM (2014) Preparation and characterization of novel polyurethanes containing 4,4′-{oxy-1,4-diphenyl bis (nitromethylidine)} diphenol schiff base diol. Polym Eng Sci 54:24–32
5. Raghu AV, Gadaginamath GS, Aminabhavi TM (2005) Synthesis and characterization of novel polyurethanes based on 1,3-bis (hydroxymethyl) benzimidazolin-2-one and 1,3-bis (hydroxymethyl) benzimidazolin-2-thione hard segments. J Appl Polym Sci 98:2236–2244
6. Raghu AV, Gadaginamath GS, Priya M (2008) Synthesis and characterization of novel polyurethanes based on N1, N4-bis [(4-hydroxyphenyl) methylene] succinohydrazide hard segment. J Appl Polym Sci 110:2315–2320
7. Keramati M, Ghasemi I, Karrabi M, Azizi H, Sabzi M (2016) Dispersion of graphene nanoplatelets in polylactic acid with the aid of a zwitterionic surfactant: evaluation of the shape memory behavior. Polym Plast Technol Eng 55:1039–1047
8. Lashgari S, Karrabi M, Ghasemi I, Azizi H, Messori M (2016) Graphene nanoplatelets dispersion in poly(l-lactic acid): preparation method and its influence on electrical, crystallinity and thermomechanical properties. Iran Polym J 25:193–202
9. Lashgari S, Karrabi M, Ghasemi I, Azizi H, Messori M, Paderni K (2016) Shape memory nanocomposite of poly(L-lactic acid)/graphene nanoplatelets triggered by infrared light and thermal heating. Exp Polym Lett 10:349–359
10. Keramati M, Ghasemi I, Karrabi M, Azizi H, Sabzi M (2016) Incorporation of surface modified graphene nanoplatelets for development of shape memory PLA nanocomposite. Fibers Polym 17:1062–1068
11. Jeong HM, Song JH, Lee SY, Kim BK (2001) Miscibility and shape memory property of poly(vinyl chloride)/thermoplastic polyurethane blends. J Mater Sci 36:5457–5463
12. Laukaitiene A, Jankauskaite V, Žukiene K, Norvydas V, Munassipov S, Janakhmetov U (2013) Investigation of polyvinyl chloride and thermoplastic polyurethane waste blend miscibility. Medziagotyra 19:397–402
13. Rashidi B, Golshan EN (2007) Investigation of compatibility and properties of polyvinyl chloride/ester-based polyurethane blends. Iran J Polym Sci Technol 20:41–48
14. Zhao X, Zhao J, Cao JP, Wang D, Hu GH, Chen F, Dang ZM (2014) Effect of the selective localization of carbon nanotubes in polystyrene/poly (vinylidene fluoride) blends on their dielectric, thermal, and mechanical properties. Mater Des 56:807–815
15. Le HH, Schoß M, Ilisch S, Gohs U, Heinrich G, Pham T, Radusch HJ (2011) CB filled EOC/EPDM blends as a shape-memory material: manufacturing, morphology and properties. Polymer 52:5858–5866
16. Jiang HJ, Cao S, Ke CB, Ma X, Zhang XP (2013) Nano-sized SiC particle reinforced NiTi alloy matrix shape memory composite. Mater Lett 100:74–77
17. Kim KT, Dao TD, Jeong HM, Anjanapura RV, Aminabhavi TM (2015) Graphene coated with alumina and its utilization as a thermal conductivity enhancer for alumina sphere/thermoplastic polyurethane composite. Mater Chem Phys 153:291–300
18. Choi SH, Kim DH, Raghu AV, Reddy KR, Lee HI, Yoon KS, Jeong HM, Kim BK (2012) Properties of graphene/waterborne polyurethane nanocomposites cast from colloidal dispersion mixtures. J Macromol Sci B 51:197–207
19. Martınez MT, Callejas MA, Benito AM, Cochet M, Seeger T, Anson A, Schreiber J, Gordon C, Marhic C, Chauvet O, Fierro JL (2003) Sensitivity of single wall carbon nanotubes to oxidative processing: structural modification, intercalation and functionalisation. Carbon 41:2247–2256
20. Hou PX, Bai S, Yang QH, Liu C, Cheng HM (2002) Multi-step purification of carbon nanotubes. Carbon 40:81–85
21. Datsyuk V, Kalyva M, Papagelis K, Parthenios J, Tasis D, Siokou A, Kallitsis I, Galiotis C (2008) Chemical oxidation of multi-walled carbon nanotubes. Carbon 46:833–840
22. Strong KL, Anderson DP, Lafdi K, Kuhn JN (2003) Purification process for single-wall carbon nanotubes. Carbon 41:1477–1488
23. Lu C, Chiu H (2006) Adsorption of zinc(II) from water with purified carbon nanotubes. Chem Eng Sci 61:1138–1145
24. Wu C, Liao H (2007) Study on the preparation and characterization of biodegradable polylactide/multi-walled carbon nanotubes nanocomposites. Polymer 48:4449–4458
25. Guojiann W, Lijuan W, Mei Z, Zhengmian C (2009) Reinforcement and toughening of poly(vinyl chloride) with poly(caprolactone) grafted carbon nanotubes. Compos A Appl Sci Manuf 40:1476–1481
26. Abdullah SA, Jumahat A, Abdullah NR, Frormann L (2012) Determination of shape fixity and shape recovery rate of carbon nanotube-filled shape memory polymer nanocomposites. Proc Eng 41:1641–1646
27. Nguyen DA, Lee YR, Raghu AV, Jeong HM, Shin CM, Kim BK (2009) Morphological and physical properties of a thermoplastic polyurethane reinforced with functionalized graphene sheet. Polym Int 58:412–417

28. Yoo HJ, Jung YC, Sahoo NG, Cho JW (2006) Polyurethane-carbon nanotube nanocomposites prepared by in-situ polymerization with electroactive shape memory. J Macromol Sci B Phys 45B:441–451

29. Wang CB, Cooper SL (1981) Morphology and properties of poly(vinyl chloride)–polyurethane blends. J Appl Polym Sci 26:2989–3006

30. Çalışır Ü, Çiçek B (2020) Synthesis of thiol-glycol-functionalized carbon nanotubes and characterization with FTIR, TEM, TGA, and NMR technics. Chem Papers 74:3293–3302

31. Luo C, Tang F, Li S (2020) Effects of multi-walled carbon nanotubes grafted polycaprolactone on crystallization behavior and thermal stability of poly(*L*-lactic acid). Acta Mater Compos Sin 37:74–81

32. Tekay E (2020) Preparation and characterization of electro-active shape memory PCL/SEBS-*g*-MA/MWCNT nanocomposites. Polymer 209:122989

33. Xiong J, Zheng Z, Qin X, Li M, Li H, Wang X (2006) The thermal and mechanical properties of a polyurethane / multi-walled carbon nanotube composite. Carbon 44:2701–2707

34. Basheer BV, George JJ, Siengchin S, Parameswaranpillai J (2020) Polymer grafted carbon nanotubes synthesis, properties, and applications: a review. Nano-struct Nano-objects 22:100429

35. Nguyen DA, Raghu AV, Choi JT, Jeong HM (2010) Properties of thermoplastic polyurethane/functionalised graphene sheet nanocomposites prepared by the in situ polymerisation method. Polym Polym Compos 18:351–358

36. Abuilaiwi FA, Laoui T, Al-Harthi M, Atieh MA (2010) Modification and functionalization of multiwalled carbon nanotube (MWCNT) via fischer esterification. Arab J Sci Eng 35:37–48

37. Arrechea S, Guerrero-Gutiérrez EM, Velásquez L, Cardona J, Posadas R, Torres KC, Díaz R, Barrientos C, García E (2020) Effect of additions of multiwall carbon nanotubes (MWCNT, MWCNT-COOH and MWCNT-Thiazol) in mechanical compression properties of a cement-based material. Materialia 19:100739

38. Osorio AG, Silveira IC, Bueno VL, Bergmann CP (2008) H_2SO_4/HNO_3/HCl-functionalization and its effect on dispersion of carbon nanotubes in aqueous media. Appl Surf Sci 255:2485–2489

39. Demma G, Martuscelli E, Zanetti A, Zorzetto M (1983) Morphology and properties of polyurethane-based blends. J Mater Sci 18:89–102

40. Azizi S, Azizi M, Sabetzadeh M (2019) The role of multiwalled carbon nanotubes in the mechanical, thermal, rheological, and electrical properties of PP/PLA/MWCNTs nanocomposites. J Compos Sci 3:64

41. Jahanmard F, Eslaminejad MB, Amani-Tehran M, Zarei F, Rezaei N, Croes M, Yavari SA (2020) Incorporation of F-MWCNTs into electrospun nanofibers regulates osteogenesis through stiffness and nanotopography. Mater Sci Eng C 106:110163

42. Frank BP, Goodwin DG Jr, Bohutskyi P, Phan DC, Lu X, Kuwama L, Bouwer EJ, Fairbrother DH (2020) Influence of polymer type and carbon nanotube properties on carbon nanotube/polymer nanocomposite biodegradation. Sci Total Environ 742:140512

43. Sabahi N, Chen W, Wang CH, Kruzic JJ, Li X (2020) A review on additive manufacturing of shape-memory materials for biomedical applications. JOMs 72:1229–1253

44. Kwiatkowska M, Pełech R, Jędrzejewska A, Moszyński D, Pełech I (2020) Different approaches to oxygen functionalization of multi-walled carbon nanotubes and their effect on mechanical and thermal properties of polyamide 12 based composites. Polymers 12:308

45. Ponnamma D, Sadasivuni KK, Strankowski M, Moldenaers P, Thomas S, Grohens Y (2013) Interrelated shape memory and Payne effect in polyurethane/graphene oxide nanocomposites. RSC Adv 3:16068–16079

46. Haghayegh M, Mir MohammadiSadeghi G, Shamayeli B (2012) Synthesis of shape memory polyurethane/nanoclay composites: chemical structure and interactions between polymer and nanoclay particles. Iran J Polym Sci Technol 25:19–30

47. Kim JT, Kim BK, Kim EY, Park HC, Jeong HM (2014) Synthesis and shape memory performance of polyurethane/graphene nanocomposites. React Funct Polym 74:16–21

48. Behl M, Lendlein A (2007) Shape-memory polymers: a review. Mater Today 10:20–28

49. Koerner H, Price G, Pearce NA, Alexander M, Vaia RA (2004) Remotely actuated polymer nanocomposites—stress-recovery of carbon-nanotube-filled thermoplastic elastomers. Nat Mater 3:115–120

50. Gu S, Yan B, Liu L, Ren J (2013) Carbon nanotube-polyurethane shape memory nanocomposites with low trigger temperature. Eur Polym J 49:3867–3877